Dielectric and Pyroelectric Properties of Lithium Hydrogen Dimalate, $LiH_3(C_4H_4O_5)_2$

Silvia Fleck * and Alarich Weiss
Institut für Physikalische Chemie, Physikalische Chemie III, Technische Hochschule Darmstadt

Z. Naturforsch. **41 a**, 1289–1296 (1986); received July 5, 1986

The dielectric constant and the pyroelectric coefficient at constant stress of 1-lithium hydrogen dimalate 1-$Li^{\oplus}(OOCCHOHCH_2COOH)^{\ominus}(HOOCCHOHCH_2COOH)$, were investigated in the temperature range $200 \leqq T/K \leqq T_d$ (decomposition temperature) and $100 \leqq T/K \leqq T_d$, respectively. The compound crystallizes in the space group $P2_1$. In the direction of the 2_1 axis ε'_{22} increases with almost constant slope with increasing temperature from 7.32 (200 K) to 8.55 (360 K). The pyroelectric coefficient p_2 shows a maximum at 152 K and a minimum at 290 K; p_2 lies between 15 $\mu C\,m^{-2}\,K^{-1}$ and 6 $\mu C\,m^{-2}\,K^{-1}$. The contribution of the lattice to the polarization was calculated on the basis of a point charge model developed from a charge distribution calculation on the INDO basis. Assuming certain lattice vibration frequencies and a harmonic oscillator model, $p_2 = f(T)$ was calculated.
Qualitatively the calculations are in satisfactory agreement with the experiment.

Introduction

Some time ago Traube [1] has studied a series of salts of 1-malic acid 1-$HOOCCH_2CHOHCOOH$ (preparation, optical measurements). The work done before 1915 is reviewed by Groth [2]. Several salts of malic acid crystallize in an acentric structure and are therefore of interest because of their physical properties such as pyroelectricity, piezoelectricity etc. For example pyroelectricity has found more and more attention recently for thermal detectors [3–5].

In this paper we report on the dielectric and pyroelectric properties of a lithium salt of malic acid which contains one lithium ion and two molecules of 1-malic acid in the formula unit. The pyroelectricity of this salt was qualitatively observed by Traube [1], who has formulated the compound as 1-$Li^{\oplus}(C_4H_5O_5)^{\ominus} \cdot 6H_2O$. The salt was identified by us by chemical analysis, mass density measurements and crystal structure determination as 1-$Li^{\oplus}(OOCCH_2CHOHCOOH)^{\ominus}(HOOCCH_2CHOHCOOH)$. In the following this formula is abbreviated as LiH_3Mal_2. The crystal structure of the compound was recently reported by Kirfel et al. [6]. Our refinement is within the limits of error in complete agreement with [6], and we shall give the details elsewhere [7]. The space group of the title compound is C_2^2–$P2_1$, with 2 formula units in the unit cell. The polar axis 2_1 is choosen as the axis b (2nd setting).

Structure determinations on salts of malic acid have been reported in recent years by Schmittler [8], Kryger and Rasmussen [9], Reed and Karipides [10], Lenstra and coworkers [11], and Seiler et al. [12].

Experimental

Preparation

LiH_3Mal_2 was prepared from commercial components (1-malic acid and lithium hydroxide) in aqueous solution. Stoichiometric amounts were used (LiOH : malic acid = 1 : 2). The composition of the crystals determined by chemical analysis is (calculated values in brackets): C: 34.81% (35.05%); H: 3.87% (4.05%).

Large single crystals (15 × 8 × 6 mm) can be grown by slow evaporation of H_2O from aqueous solution at 290 K. Identification of the crystal axes and faces was made by comparison of the optical measurements with the crystal structure data. The habitus of the crystal is shown in Fig. 1; the finding is in good agreement with the optical measurements of Traube [1].

---

* Part of the Dr.-Ing. thesis of Silvia Fleck, Darmstadt.

Reprint requests to Prof. Dr. Al. Weiss, Institut f. Physikal. Chemie, Physikalische Chemie III, Petersenstr. 20, D-6100 Darmstadt, West Germany.

0340-4811 / 86 / 1100-1289 $ 01.30/0. – Please order a reprint rather than making your own copy.

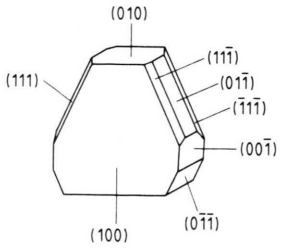

Fig. 1. Habitus of 1-lithium hydrogen dimalate, $Li^{\oplus}(^{\ominus}OOCCHOHCH_2COOH)(HOOCCHOHCH_2COOH)$.

By differential thermal analysis, DTA, a decomposition point, $T_d = 353$ K, was detected in the range $77 \leqq T/K \leqq 400$. No other thermal anomaly was found in this temperature range.

For the measurements of the dielectric constant and of the pyroelectric coefficient, plates of LiH_3Mal_2 were cut parallel to (010) with a wire saw. The faces (010) and (0$\bar{1}$0) were polished and painted with an air drying silver paste. In this way single crystal capacitors with an area $12 \leqq A/mm^2 \leqq 35$ and a thickness $0.5 \leqq d/mm \leqq 1$, filled with the single crystal dielectricum LiH_3Mal_2 were obtained.

Measurement of the Dielectric Properties

The impedance of the single crystal capacitor was measured in the temperature range from 200 K to the decomposition temperature T_d, using a bridge method (Wayne-Kerr Universal Bridge B224, operating at audio frequency, range $500 \leqq \nu/Hz \leqq 20000$). The temperature of the sample was controlled by thermostates with methanol or oil as carrier liquids. The measurement of the actual temperature at the sample site by thermocouples Cu/Constantan was accurate to ± 0.5 K. The dielectric measurements were limited in accuracy by the determination of the crystal area and its thickness to $\pm 3\%$.

Measurement of the Pyroelectric Coefficient at Constant Stress

For the measurement of the pyroelectric coefficient at constant stress the single crystal capacitor was inserted between silver electrodes into a cryostat similar to that described by Lang et al. [13]. The temperature at the site of the sample was determined by thermocouples, see above (accuracy ± 1 K). The pyroelectric voltage was measured using both the method of constant temperature change and the method of sinusoidal temperature oscillation. The experimental arrangements have been already described [14]. The accuracy of the pyroelectric coefficient obtained is 10%. The measurements were repeated in the temperature range $100 \leqq T/K \leqq T_d$ for several (010)-plates cutted from different single crystals.

Theory

Quantummechanical Calculation of the Charge Distribution in Crystalline LiH_3Mal_2

In order to discuss the temperature dependence of the pyroelectric coefficient in terms of microscopic properties, it is necessary to calculate the magnitude and the direction of the dipole moment. We have studied the charge distribution and the electric dipole moment of LiH_3Mal_2 in the solid state. The calculations are based on a semiempirical molecular orbital model by linear combination of atomic orbitals (MO-LCAO) in the version of intermediate neglect of differential overlap (INDO) [15]. The solid state effects have been simulated by a self consistent electrostatic field approach (SCEF), which leads to an approximate expression for the interaction energy between a selected reference molecule and its neighbours [16]. The employed SCEF model is thus suitable for the investigation of intermolecular interactions which are governed by Coulomb forces. Such interactions are predominant in LiH_3Mal_2, with strong hydrogen bonds in the solid state and with isolated lithium ions. More details of the used SCEF model will be published separately.

In the numerical SCEF-INDO calculations we adopted the experimental crystal structure parameters for the asymmetric unit ($HOOCCH_2CHOHCOOH$) $Li^{\oplus}(^{\ominus}OOCCHOHCH_2COOH)$, using the atomic numbering scheme displayed in Figure 2. Only such neighbouring asymmetric units (N) are employed in the electrostatic field approach, which are coupled to the reference system via hydrogen bonds or via electrostatic contacts to $Li^{\oplus}$. Our calculations are carried out with one reference unit and six neighbouring ones which are treated as point charge distributions to simulate the electrostatic field.

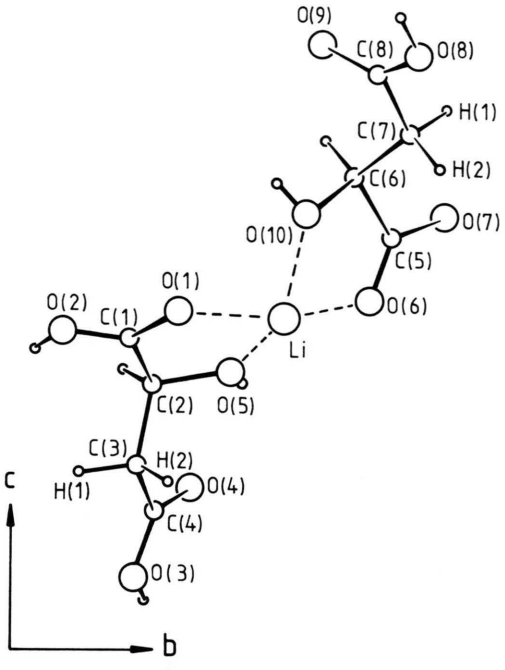

Fig. 2. Atomic numbering scheme of the asymmetric unit in the elementary cell of LiH_3Mal_2.

In Fig. 3 a projection of the crystal structure along the [100]-axis is shown. The atoms of the reference unit R are symbolized by filled circles and the six neighbours considered in the SCEF are given by shadowed atoms. The six neighbours considered are held together by electrostatic interactions with the $Li^{\oplus}$ ions and by hydrogen bonds. Each $Li^{\oplus}$ is pentacoordinated by oxygen, where four oxygens of the coordination sphere belong to the same asymmetric unit and one belongs to a second. On the level ($0 \leqq x/a \leqq 1$) the hydrogen bonds connect the formula units preferentially in the direction of the [010]-axis. A second set of hydrogen bonds connects formula units preferentially within the plane (010). The neighbouring molecules V and VI are above III and below IV, respectively.

Temperature Dependence of the Pyroelectric Coefficient

The temperature dependence of the pyroelectric coefficient at constant stress can be calculated as a function of the dielectric constant ε and the angle δ

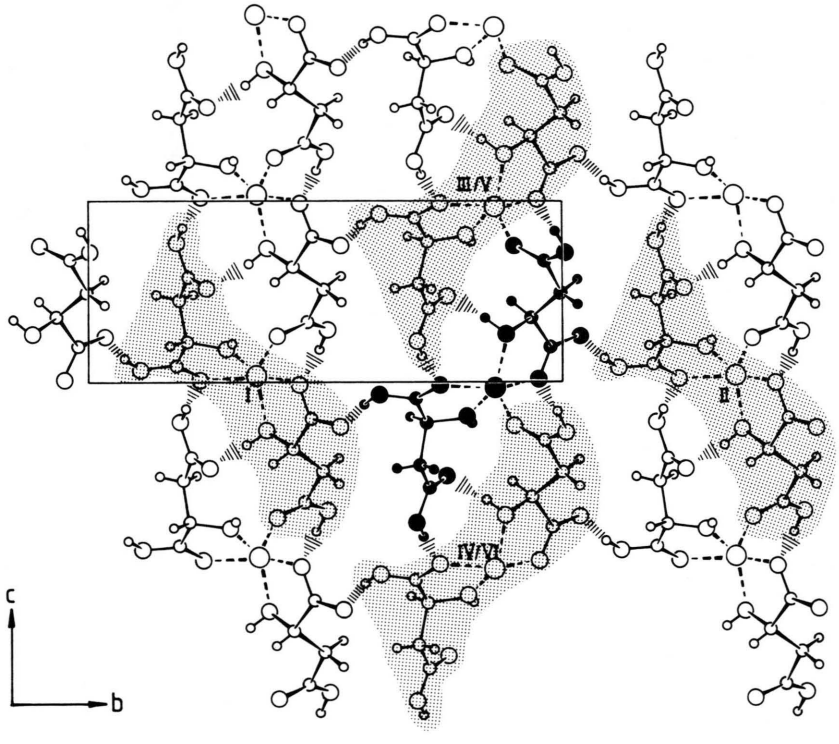

Fig. 3. Projection of the crystal structure along the axis [100]. Fully drawn is the reference molecule R. The shadowed molecules are the neighbours N considered in the INDO-SCEF calculations (see text).

between the direction of the polarization $\boldsymbol{P}$ and the dipole moment $\boldsymbol{\mu}$. Following Mopsik and Broadhurst [17], a dielectricum can be characterized by dipoles with a permanent moment $\boldsymbol{\mu}$ and polarizability α, librating with a temperature dependent amplitude. Due to the polarizability the total moment $\boldsymbol{m}$ depends on the internal electric field $\boldsymbol{E}_i$:

$$\boldsymbol{m} = \boldsymbol{\mu} + \alpha \boldsymbol{E}_i , \tag{1}$$

and the component of $\boldsymbol{m}$ in the direction of the polarization, m_P, is

$$m_P = \mu \cdot \cos\delta + \alpha E_{i,P} . \tag{2}$$

The internal field, $\boldsymbol{E}_i$, is composed of different parts. Those contributions to $\boldsymbol{E}_i$ which come from charges outside the crystal and from its surfaces, cancel each other if we regard an electroded sample with shortened electrodes. Another part of the internal field is the so called Lorentz-field, $\boldsymbol{E}_L$ [18]. It is the electric field arising from the polarization charge on a spherical surface which is formed if a spherical hole is carved out from a homogeneously polarized dielectric medium. It can be described by Lorentz's equation

$$\boldsymbol{E}_L = \frac{1}{3\varepsilon_0} \boldsymbol{P} , \tag{3}$$

where the permittivity constant $\varepsilon_0 = 8.859 \cdot 10^{-12}$ $CV^{-1}\,m^{-1}$.

For a cubic crystal, at the site of a given dipole R the contributions to $\boldsymbol{E}_i$ arising from dipoles N are zero.

To treat noncubic crystals we extend the theory and apply it to a monoclinic system, e.g. the LiH_3Mal_2 crystal which is studied here. In such a case the field $\boldsymbol{E}_N$ of the neighbouring molecules N has to be taken into account. $\boldsymbol{E}_N$ is calculated by a model which treats the neighbouring molecules as charge distributions based on the atomic net charges found by the SCEF-INDO approach. The field of the charge distribution at the center of the reference molecule R (= asymmetric unit R) is found from

$$\boldsymbol{E}_N = \frac{1}{4\pi\varepsilon_0} \sum_N \sum_j \frac{q_j \boldsymbol{r}_j}{r_j^3} \equiv \frac{1}{4\pi\varepsilon_0} \boldsymbol{S}_N , \tag{4}$$

where q_j = charge at the atom j, $\boldsymbol{r}_j$ = radius vector from the atom j in the neighbouring unit N to the center of the asymmetric unit R. The component of $\boldsymbol{E}_N$ in the direction of the polarization, $E_{N,P}$, is given by

$$E_{N,P} = \frac{1}{4\pi\varepsilon_0} S_N \cdot \cos\beta , \tag{5}$$

with β = angle between $\boldsymbol{P}$ and $\boldsymbol{E}_N$.

The internal field in the direction of the polarization, $E_{i,P}$, is

$$E_{i,P} = E_L + E_{N,P} = \frac{1}{3\varepsilon_0} P + \frac{1}{4\pi\varepsilon_0} S_N \cdot \cos\beta . \tag{6}$$

The total polarization P can be found from (2) by multiplication with the number of molecules per unit volume $N_A/\bar{V}$ as

$$P = \frac{N_A}{\bar{V}} (\mu \cos\delta + \alpha E_{i,P}) , \tag{7}$$

with N_A = Avogadro number and $\bar{V}$ = molar volume.

LiH_3Mal_2 crystallizes in the space group C_2^2–$P2_1$ and we choose here the setting of [010] as the axis 2_1. In this case the direction of polarization is uniquely the direction of the crystallographic b-axis. The dielectric constant in the direction of the polarization is then $\varepsilon_P = \varepsilon_{22}$. We can calculate the polarizability from the dielectric constant by the Clausius-Mossotti relation:

$$\alpha = \frac{\bar{V}}{N_A} \cdot 3\varepsilon_0 \cdot \frac{(\varepsilon_P - 1)}{(\varepsilon_P + 2)} . \tag{8}$$

Combination of (6), (7), and (8) leads to

$$P = \frac{N_A}{3\bar{V}} (\varepsilon_P + 2)\, \mu \cos\delta + \frac{1}{4\pi} (\varepsilon_P - 1)\, S_N \cdot \cos\beta . \tag{9}$$

The pyroelectric coefficient at constant stress, p_2, is found by differentiation of (9) with respect to temperature. This means that we have to take into account:

1. Change of the polarization caused by changes of the number of molecules per unit volume with temperature,
2. changes of the internal electric field with temperature resulting in a change of the induced dipole moment, and
3. changes of $\cos\delta$ and $\cos\beta$ with temperature, caused by librational motions.

This can be formulated as

$$\frac{\partial P}{\partial T} = \left(\frac{\partial P}{\partial T}\right)_{\delta,\beta,\varepsilon_P} + \left(\frac{\partial P}{\partial T}\right)_{V,\beta,\varepsilon_P} + \left(\frac{\partial P}{\partial T}\right)_{V,\delta,\varepsilon_P} + \left(\frac{\partial P}{\partial T}\right)_{V,\delta,\beta} , \tag{10}$$

$$\frac{\partial P}{\partial T} = -\frac{N_A}{3\bar{V}^2}(\varepsilon_P + 2)\,\mu\cos\delta\frac{\partial \bar{V}}{\partial T} + \frac{N_A}{3\bar{V}}(\varepsilon_P + 2)\,\mu\frac{\partial\cos\delta}{\partial T} + \frac{1}{4\pi}(\varepsilon_P - 1)\,S_N\frac{\partial\cos\beta}{\partial T} + \left(\frac{N_A}{3\bar{V}}\,\mu\cos\delta + \frac{1}{4\pi}S_N\cdot\cos\beta\right)\frac{\partial\varepsilon_P}{\partial T}. \quad (11)$$

In good approximation the first term in (11) may be neglected since $\partial\bar{V}/\partial T$ should be continuous over the whole temperature range studied (no phase transition was observed) and $\Delta\bar{V}/\Delta T$ ($\Delta T \approx 200$ K) should be less than 1%. The other three terms in (11) are numerically comparable and have to be fully considered in an estimation of the pyroelectric coefficient. In [14] we have made a more restricted approximation to the problem.

Results

Our refinement of the crystal structure of LiH_3Mal_2 will not be reported here. For details see [7]. The calculations of the pyroelectric coefficient will be the same by using either the results of [6] or of [7].

The Dielectric Constant ε_{22}

The variation of the dielectric constant in the direction of the polar axis 2_1 at a fixed frequency of 1.592 kHz is shown as a function of temperature in Figure 4. Both components of $\varepsilon_{22} = \varepsilon'_{22} - i\varepsilon''_{22}$ are given. ε'_{22} increases almost linearly with increasing temperature over the range from 200 K to the decomposition at 353 K. There is a very slight change in slope near 300 K. The pronounced increase of ε'_{22} above 380 K is due to the set in of decomposition. ε''_{22} is very small, less than 0.1 below 350 K, and a strong increase is observed at $T \approx$ 380 K, not unexpected for a decomposing solid. Some numerical data are given in Table 1.

The Pyroelectric Coefficient p_2

For the space group C_2^2–$P2_1$, $2_1 \parallel b$, the pyroelectric coefficient has the form $(0, p_2, 0)$. p_2 was measured on crystal plates parallel to (010) as a function of temperature and the results are shown in Figure 5. Points marked by squares are measured with increasing temperature; circles denote measurements with falling temperature, while the triangles stand for experiments with sinoidal temperature oscillation.

The complex dependence of p_2 on temperature shows a maximum at 152 K followed by a decrease in the range $150 \leqq T/\mathrm{K} \leqq 270$ until a minimum at ≈ 290 K is reached. Thereafter a slight increase up to 340 K is observed, which ends in sharp decrease while decomposition starts.

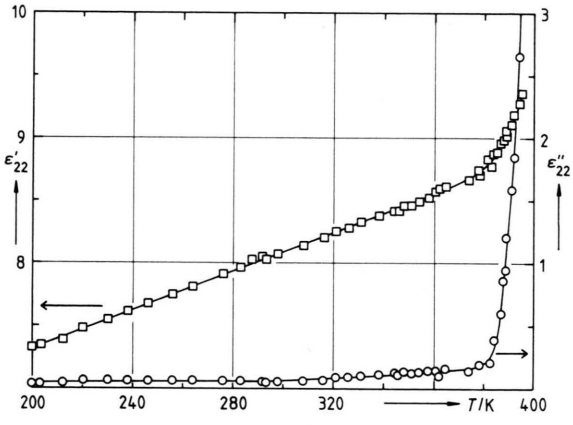

Fig. 4. Dielectric constant ε'_{22}, ε''_{22} in the direction of the polar axis 2_1 as function of temperature.

Table 1. Pyroelectric coefficient p_2 and dielectric constant ε_{22} of LiH_3Mal_2 at different temperatures.

T/K	$p_2/(\mu\mathrm{C\,m^{-2}\,K^{-1}})$	ε_{22}
100	13.0	
120	13.6	
140	14.0	
160	13.9	
180	12.7	
200	11.2	7.32
220	9.6	7.46
240	8.1	7.63
260	6.9	7.77
280	6.1	7.94
300	6.1	8.08
320	6.6	8.24
340	7.0	8.40
360	2.9	8.57

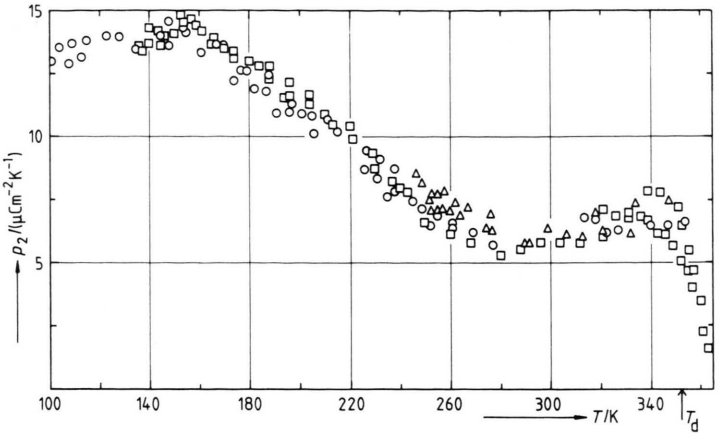

Fig. 5. Pyroelectric coefficient p_2 as function of temperature.

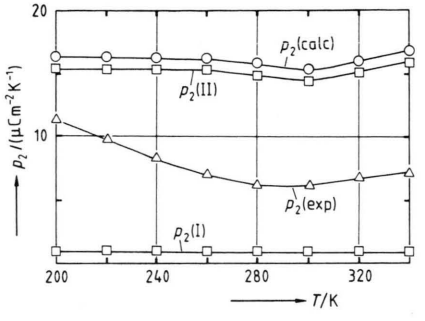

Fig. 6. Calculated pyroelectric coefficients, p_2(I), p_2(II), and p_2(calc), as function of temperature, together with p_2(exp).

Table 2. Atomic net charges from SCEF-INDO.

C(1)	0.79	Li	0.18
O(1)	− 0.53	C(5)	0.86
O(2)	− 0.58	O(6)	− 0.70
H(O2)	0.43	O(7)	− 0.85
C(2)	0.22	C(6)	0.17
H(C2)	0.08	H(C6)	0.07
O(5)	− 0.45	O(10)	− 0.48
H(O5)	0.39	H(O10)	0.35
C(3)	− 0.20	C(7)	− 0.19
H(1, C3)	0.13	H(1, C7)	0.10
H(2, C3)	0.11	H(2, C7)	0.13
C(4)	0.81	C(8)	0.86
O(3)	− 0.58	O(8)	− 0.63
H(O3)	0.37	H(O8)	0.46
O(4)	− 0.61	O(9)	− 0.71

Electric Dipole Moment and Net Charges from the SCEF-INDO Calculations

The net charges resulting from the quantum chemical calculations by application of the above mentioned approach are given in Table 2. The calculation of the resulting dipole moment gives $55.61 \cdot 10^{-30}$ C · m (16.66 D) with a component of $-51.94 \cdot 10^{-30}$ C · m (− 15.36 D) in the [010]-direction. Because of the symmetry of the crystal there is an overall compensation of components of $\boldsymbol{\mu}$ in the (ac)-plane.

Discussion

The pronounced changes of the pyroelectric coefficient p_2 with temperature are somewhat unusual for a solid without a phase transition in the temperature range studied. The question arises about a theoretical interpretation of the function $p_2 = f(T)$. In (11) the dependence of p_2 on the different temperature sensitive parameters $\varepsilon_{22} \cong \varepsilon_P$, V, δ, and β is given.

The numerical value of $N_A/\bar{V}$ in (11) can easily be obtained from the relation $\bar{V} = M/\varrho$, with ϱ = mass density = 1.59 Mgm^{-3} for LiH_3Mal_2 at room temperature and M = molar mass = 274.113 g · mol^{-1}.

The permant dipole moment $\boldsymbol{\mu}$ was calculated by SCEF-INDO to be $-51.94 \cdot 10^{-30}$ C · m in the direction of the axis 2_1. The electric field $E_{N,P}$ given by (4) and (5) is gaind from the charge distribution found by the SCEF-INDO calculations. Numbers are given in Table 2. To take the neighbouring molecules into account, the point charges of 42

neighbouring molecules were considered. A value for $(4\pi)^{-1} S_N \cos\beta$ of $0.06242\,\mathrm{C \cdot m^{-2}}$ in the direction [010] is calculated.

In (11) there are two temperature dependent quantities ε_{22} and $\partial\varepsilon_{22}/\partial T$. We have deduced these quantities from Table 1 and Figure 4. Furthermore we can assume that the change of $\cos\beta$ and the change of $\cos\delta$ with temperature are coupled because the variation of the dipole moment $\boldsymbol{\mu}$ and of the electric field of the neighbouring molecules $\boldsymbol{E}_N$ has the same origin, namely the temperature dependence of the atomic displacements; we can write $\partial \cos\beta/\partial T = -\partial \cos\delta/\partial T$.

Introducing all the relations discussed and the numbers given above, (11) reduces to

$$p_2 = \{0.06048\,(\varepsilon_{22}+2) - 0.06242\,(\varepsilon_{22}-1)\}\,\frac{\partial \cos\delta}{\partial T} + 0.001935\,\frac{\partial \varepsilon_{22}}{\partial T} = p_2(\mathrm{I}) + p_2(\mathrm{II})\,. \tag{12}$$

According to [16] a reasonable evaluation of $\partial \cos\delta/\partial T$, e.g. the variation of the angle δ between the molecular dipole direction and the polar axis of the crystal with temperature is given by

$$\partial \cos\delta/\partial T = -\cos\delta \cdot J_1(\varphi)\,\partial\varphi/\partial T\,. \tag{13}$$

$J_1(\varphi)$ is the Bessel function of first kind and first order, and (φ) is the amplitude of the dipole oscillations. For a classical harmonic oscillator the mean squares amplitude of vibration is given by

$$\langle\varphi^2\rangle = \frac{kT}{2\pi^2 \nu^2 I}\,, \tag{14}$$

where I is the moment of inertia and ν the frequency of the lattice vibrations in the Einstein model. From (14) we find

$$\frac{\partial \cos\delta}{\partial T} = -\cos\delta \cdot J_1(\varphi) \cdot \left(\frac{k}{8\pi^2 \nu^2 I T}\right)^{1/2}\,. \tag{15}$$

No experimental data for the lattice vibrations of LiH_3Mal_2 are known. However, for malic acid and ammonium hydrogen malate Raman spectroscopical investigations are found in [19] and [20], respectively. In first approximation we can compare these lattice vibration modes with the lattice frequencies of LiH_3Mal_2. For malic acid the lowest lattice vibration frequency is given at $334\,\mathrm{cm^{-1}}$ [19] and for ammonium hydrogen malate at $65\,\mathrm{cm^{-1}}$ [20]. We now assume that for lattice vibrations in LiH_3Mal_2 the molecule $HOOCCH_2CHOHCOOH$ and the ion ($^{\ominus}OOCCHOHCH_2COOH$) are important. The main principal axes of both the malic acid molecule and the malate ion (1-) are nearly perpendicular to the axis 2_1 (see Figure 3), the moment of inertia around the 2_1 axis of the molecule or ion being $9.33 \cdot 10^{-45}\,\mathrm{kg\,m^2}$. We have calculated p_2 as a function of temperature using the frequency, $\tilde{\nu} = 65\,\mathrm{cm^{-1}}$, and the frequency model [17]. The calculated curves are shown in Fig. 6 together with the experimental results.

It can be seen from (12) that the dielectric constant ε_{22} and its temperature dependence play an important role in the temperature dependence of p_2. Figure 4 shows that ε_{22} increases appreciably with temperature. However, the change of ε_{22} with T is almost constant over a wide range of temperature. The contribution of the second term in (12) which introduces $\partial\varepsilon_{22}/\partial T$ into $p_2(T)$ is shown in Fig. 6 and it is marked by $p_2(\mathrm{II})$. One can see a slight change of $p_2(\mathrm{II})$ above 260 K which leads to a weak minimum in $p_2(\mathrm{II}) = f(T)$.

The first term in (12) calculated with the observed vibrational frequency is shown by $p_2(\mathrm{I})$. Adding up terms I and II leads to the curve $p_2(\mathrm{calc})$.

Qualitative agreement between $p_2(\mathrm{exp}) = f(T)$ and $p_2(\mathrm{calc})$, which contains the vibrational frequency $\tilde{\nu}(1) = 65\,\mathrm{cm^{-1}}$ is given. We do not expect a quantitative agreement because the constants given in (12) are calculated from differences of large numbers and therefore large uncertainties are introduced. However, the slope of curves $p_2(\mathrm{calc})$ and $p_2(\mathrm{exp})$ is, in comparison, satisfactory. In the experiment we found a maximum of p_2 at ≈ 150 K and a decrease of p_2 below this temperature. Unfortunately we do not have ε_{22} data below 200 K. However, one can speculate that ε_{22} should have a temperature coefficient decreasing with decreasing temperature below 200 K. This would lead via the term II in (12) to a decrease in p_2.

Acknowledgement

We are grateful to the Stiftung Volkswagenwerk for support of this work. We also thank Dr. M. C. Böhm for the INDO-program. The crystal structure work was done in cooperation with Dr. H. Paulus.

[1] H. Traube, Z. Krist. **31,** 160 (1899).
[2] P. Groth, Chemische Kristallographie, III. Teil, 290 (1910), Engelmann-Verlag, Leipzig.
[3] H. P. Beerman, Infrared Phys. **15,** 225 (1975).
[4] E. H. Putley, in: Topics in Applied Physics, **19,** Optical and Infrared Detectors, Springer-Verlag, Berlin 1977.
[5] S. G. Porter, Ferroelec. **33,** 193 (1981).
[6] A. Kirfel, G. Will, K. Recker, F. Wallrafen, and G. Zhangshou, Z. Krist. **165,** 117 (1983).
[7] S. Fleck, Dissertation (Dr.-Ing.), Darmstadt.
[8] H. Schmittler, Acta Crystallogr. **B24,** 983 (1968).
[9] L. Kryger and S. E. Rasmussen, Acta Chem. Scand. **26,** 2349 (1972).
[10] A. T. Reed and A. Karipides, Acta Crystallogr. **B32,** 2085 (1976).
[11] A. T. H. Lenstra and W. van de Mieroop, Bull. Soc. Chim. Belg. **85,** 727 (1976); W. Versichel, W. van de Mieroop, and A. T. H. Lenstra, Acta Crystallogr. **B34,** 2643 (1978); W. van Havere and A. T. H. Lenstra, Bull. Soc. Chim. Belg. **87,** 419 (1978), Acta Crystallogr. **B36,** 1483 (1980), Bull. Soc. Chim. Belg. **89,** 427 (1980); A. T. H. Lenstra and W. van Havere, Acta Crystallogr. **B36,** 156 (1980); W. van Havere, A. T. H. Lenstra, and H. J. Geise, Acta Crystallogr. **B36,** 3117 (1980); J. F. J. van Loock, M. van Hooste, and A. T. H. Lenstra, Bull. Soc. Chim. Belg. **90,** 155 (1981); H. J. Geise, J. F. J. van Loock, and A. T. H. Lenstra, Acta Crystallogr. **C39,** 69 (1983); H. M. Doesburg and A. T. H. Lenstra, Bull. Soc. Chim. Belg. **92,** 249 (1983); A. T. H. Lenstra and J. Diller, Bull. Soc. Chim. Belg. **92,** 257 (1983); W. K. L. van Havere, P. T. Beurskens, and A. T. H. Lenstra, J. Crystallogr. Spectrosc. Res. **15,** 45 (1985).
[12] P. Seiler, B. Martinoni, and J. P. Dunitz, Nature London **309,** 435 (1984).
[13] S. B. Lang, S. A. Shaw, L. H. Rice, and K. D. Timmerhaus, Rev. Sci. Instrum. **40,** 274 (1969).
[14] T. Asaji and Al. Weiss, Z. Naturforsch. **40a,** 567 (1985).
[15] J. A. Pople and D. L. Beveridge, Approximate Molecular Orbital Theory, McGraw-Hill, New York 1970.
[16] M. C. Böhm, Physica **124B,** 327 (1984).
[17] F. J. Mopsik and M. G. Broadhurst, J. Appl. Phys. **46,** 4202 (1975).
[18] G. J. F. Böttcher, Theory of Electric Polarization, Vol. I and II, Elsevier Scientific Publishing Company, Amsterdam 1973.
[19] M. Thoedoresco, C. R. Acad. Sci. Paris **274,** 169 (1942).
[20] T. S. Krishnan, Pr. Indian Acad. [A] **37,** 415 (1953).